The mechanics of state-dependent neural correlations

Brent Doiron[1,2], Ashok Litwin-Kumar[1–3], Robert Rosenbaum[1,2,4,5], Gabriel K Ocker[1,2,6] & Krešimir Josić[7,8]

Simultaneous recordings from large neural populations are becoming increasingly common. An important feature of population activity is the trial-to-trial correlated fluctuation of spike train outputs from recorded neuron pairs. Similar to the firing rate of single neurons, correlated activity can be modulated by a number of factors, from changes in arousal and attentional state to learning and task engagement. However, the physiological mechanisms that underlie these changes are not fully understood. We review recent theoretical results that identify three separate mechanisms that modulate spike train correlations: changes in input correlations, internal fluctuations and the transfer function of single neurons. We first examine these mechanisms in feedforward pathways and then show how the same approach can explain the modulation of correlations in recurrent networks. Such mechanistic constraints on the modulation of population activity will be important in statistical analyses of high-dimensional neural data.

A major challenge in systems neuroscience is understanding the patterns of neural activity that support sensory processing[1], memory[2], decision-making[3] and cognition[4]. This activity emerges from interactions between neurons[5], as well as bottom-up sensory and top-down modulatory inputs[6]. Determining the physiological basis of these activity patterns will provide constraints on theories of neural computation, as well as bridges between physiology and cognition.

Different statistical approaches have been used to uncover important features of neuronal activity, such as the functional coupling in a network[7], the dimensionality of population responses[8] and their variability[9–11]. Although these approaches identify the essential statistical features of large-scale network activity, they give little insight into the physiological causes of the observed activity patterns. Moreover, the high dimensionality and limited amount of available data obtained from neural recordings require the development of new statistical approaches[12,13]. As recordings from larger and larger groups of neurons become more common[14], identifying constraints on the activity will become essential. Computational models that capture the essential biophysical properties of actual neurons can be better constrained and interpreted than models that make no assumption about the dynamics of individual units and their interactions.

Mechanistic models have long been used to understand the receptive field organization and trial-averaged dynamics of single neuron responses. Most famously, Hubel and Wiesel postulated the structure of thalamic projections to visual cortex from single neuron firing responses to bars of light[15]. Others have used mechanistic models to examine the effect of feedforward[16] and recurrent[17,18] neural architectures on stimulus selectivity, providing targeted predictions for subsequent experimental studies of vision[19,20] and other modalities[21,22]. This approach is not restricted to sensory areas in which neural responses are easily affected by changes in stimuli. For example, there has been extensive work in building circuit models of persistent activity in prefrontal cortex during working memory tasks[23] and the formation of grid cell responses in hippocampus[24], all replicating trial-averaged single neuron responses. We propose to extend this modeling approach by outlining how specific biophysical aspects of cellular and circuit structure can explain the variability of neuronal response.

Of particular interest is the trial-to-trial covariability between the spiking activity from simultaneously recorded neuron pairs. These noise correlations provide a simple and robust measure of the internal coherence of neural activity[25]. There is a vibrant debate about how noise correlations affect neural coding[26–29]. In this review, however, we focus on the relation between noise correlations and underlying physiology of the network.

Noise correlations are frequently attributed to the presence of common afferent projections to a neuron pair[30]. A variety of mechanisms, however, can lead to correlated neural responses. On the one hand, direct common projections are not required if the presynaptic ensembles are themselves correlated[31]. On the other hand, correlations from shared excitatory and inhibitory projections can cancel, resulting in low net correlations[32]. Correlations can also reflect local recurrent connectivity[33–35] or feedforward inputs such as those induced by fluctuations in bottom-up or top-down projections[36]. Finally, the cellular nonlinearities that transfer input currents to spike outputs are also important in shaping neural correlations[37–39]. It is this diversity in the causes of noise correlations that make them challenging to study from a mechanistic perspective.

[1]Department of Mathematics, University of Pittsburgh, Pittsburgh, Pennsylvania, USA. [2]Center for the Neural Basis of Cognition, Pittsburgh, Pennsylvania, USA. [3]Center for Theoretical Neuroscience, Columbia University, New York, New York, USA. [4]Department of Applied and Computational Mathematics and Statistics, University of Notre Dame, Notre Dame, Indiana, USA. [5]Interdisciplinary Center for Network Science and Applications, University of Notre Dame, Notre Dame, Indiana, USA. [6]Allen Institute for Brain Science, Seattle, Washington, USA. [7]Department of Mathematics, University of Houston, Houston, Texas, USA. [8]Department of Biology and Biochemistry, University of Houston, Houston, Texas, USA. Correspondence should be addressed to B.D. (bdoiron@pitt.edu).

An often-used strategy in systems neuroscience is to record neural activity under different neural states. State comparisons have been made between spontaneous and stimulus-evoked neural activity[40], when attention is directed in or outside the receptive field of a population[41], different levels of arousal[42], and active versus passive sensory acquisition[43]. State modulation is essential for understanding neural activity that is specific to a certain neural computation. It also serves another purpose: it offers important clues about the circuit and cellular mechanisms underlying collective neural activity. Different mechanisms could explain the correlations observed under a single state. However, only some of these mechanisms will be consistent with observations from multiple states.

We begin our review with a partial listing of examples of state-dependent modulation of neural correlations. We next synthesize several theoretical results into one general framework that includes three mechanisms of correlation modulation: pre-synaptic correlations, internal fluctuations and neural transfer. We explore these distinct mechanisms separately using a feedforward circuit model, highlighting their differences. We finish by discussing how these insights can inform the analysis of correlation modulation in recurrent networks, where several mechanisms can be simultaneously engaged. Our review highlights how modulations in neural correlations could provide a window into the physiology that underlies state-dependent changes in the nervous system.

Modulation of neuronal correlations

Simultaneous recordings from large populations of neurons are becoming commonplace in systems neuroscience[14]. Consider two spike trains from the kth trial of such an experiment, $y_1^k(t) = \sum_m \delta(t - t_{1m}^k)$ and $y_2^k(t) = \sum_m \delta(t - t_{2m}^k)$ where the Dirac delta function $\delta(t - t_{im}^k)$ represents the mth spike from neuron i. The spike count correlation coefficient[25,44] between the two spike trains is

$$\rho(n_1^k, n_2^k) = \frac{Cov(n_1^k, n_2^k)}{\sqrt{Var(n_1^k)Var(n_2^k)}}$$

Here $n_i^k = \int_0^T y_i^k(t)dt$ is the random spike count computed over a duration T on trial k, and $Cov(n_1^k, n_2^k)$ and $Var(n_i^k)$ denote the covariance and variance over trials, respectively. When ρ appears without a subscript it always refers to output spike correlations. Over small durations ($T \sim 1-10$ ms), ρ measures spike train synchrony, whereas, over long durations ($T \sim 100-1,000$ ms), it captures shared fluctuations in the firing rates of the two neurons over trials.

A growing list of studies show large heterogeneity in correlations measured across the nervous system, as well as from neuron pairs in the same brain region[25,45–47]. Nevertheless, the average correlation coefficient across paired spike trains is typically small, ranging from 0.05 to 0.3 depending on the brain region, brain state and joint stimulus preference of the neuron pair[25,45,48]. Here we primarily consider long-timescale correlations, although our general framework is applicable to arbitrary time windows.

In this Review, we consider correlation changes induced by a broadly defined state change of the nervous system (**Box 1**). We present a partial list of examples in **Table 1**, with each entry describing two states, which show that ρ can be modulated considerably in different animals, brain regions and cognitive contexts.

In sum, the diversity in the conditions and states in which modulations in correlation occurs suggests that distinct physiological mechanisms may be responsible. We next present a unified framework to discuss and compare a number of mechanisms that can impact the correlation coefficient, ρ, as well as how it is modulated across brain states.

Central framework for correlation modulation

Biological neural circuits consist of neurons belonging to a variety of cell classes wired in complex ways. It is tempting to try to infer the structure of these circuits and the physiological properties of neurons in them from multicellular recordings from subsets of neurons. Such an approach is fraught with difficulties[49], many of which are a result of the fact that only part of the population is observed. Here we describe an alternative strategy that is more modest in scope, but provides a general framework for discussing how modulations in spiking correlations depend on biophysical changes in the underlying circuit to which the neurons belong.

To start, we consider a pair of simultaneously recorded neurons that are members of a larger, yet unknown, neural circuit (**Fig. 1**). To simplify our analysis, we assume that neurons in the pair are not directly coupled (although this is not required for our treatment). Using this assumption, we explore how the cellular properties of the postsynaptic neurons, and those of the presynaptic circuit that drives them, influence correlation transfer.

On trial k of the experiment, neuron i of our pair ($i = 1$ or 2) responds to its afferent inputs, $x_i^k(t)$, with n_i^k spikes over the window T. We consider values of T that are much larger than the synaptic and membrane timescale of the neurons, thereby not explicitly measuring the fine temporal structure of the spike trains. For simplicity, we assume that $Var(n_1) = Var(n_2) = Var(n)$, so that the correlation coefficient is $\rho = Cov(n_1, n_2)/Var(n)$.

The two neurons do not interact directly, so $\rho \neq 0$ implies that the presynaptic inputs to the neurons, $x_1(t)$ and $x_2(t)$, are themselves correlated. We quantify this correlation using the input covariance

$$Cov(\hat{x}_1, \hat{x}_2),$$

between the integrated synaptic inputs,

$$\hat{x}_i^k = \int_0^T x_i^k(t)dt.$$

When the input covariance is small we can use the linear approximation

$$Cov(n_1, n_2) \approx L^2 Cov(\hat{x}_1, \hat{x}_2) \qquad (1)$$

to relate input and output covariance[37]. Here $L_1 = L_2 = L$ is the linear response of the target neuron[50,51]. Briefly, for weak common fluctuations, $s(t)$, we have $\langle n_i \rangle \approx \langle n_{i0} \rangle + L\hat{s}$, where $\langle \cdot \rangle$ denotes the expectation over trials, $\langle n_{i0} \rangle$ is the mean spike count of the of neuron i at its operating point (defined by $s = 0$), and $\hat{s} = \int_0^T s(t)dt$. The common fluctuations then simply perturb the neuron pair's joint activity about an operational point (where $Cov(n_{10}, n_{20}) = 0$). If the operating point changes (say through a modulation), the linear approximation may change L, but equation (1) remains valid. However, if perturbations are too large, this linear approximation can break down,

---

Box 1 Neural state

The operating state of the brain, or simply state, refers to the context under which neural activity is recorded. This includes several possibilities. The cognitive state is determined by an animal's level of arousal, attentional focus or degree of engagement in a task. In the absence of a stimulus or task, the neural network is in the spontaneous state, as opposed to an evoked state. Stimuli that do not directly drive a neuron, yet recruit a non-classical surround, can change the processing state of a neuron. A change in stimulus features in a neuron's receptive field may change its firing rate. However, it does not change the context under which the neural activity is observed, and hence such stimulus features do not determine a state.

Table 1 Examples of state-dependent modulation of neural correlation ρ

System	Modulation	Window length T	ρ^B/ρ^A	References
Extracellularly recorded spike trains				
Electrosensory (fish)	Spatially broad (A) versus compact (B) stimuli	50 ms	0.68	132
V4 (macaque)	Unattended (A) versus attended (B) (spatial)	200 ms, 100 ms	0.70, 0.66	96,133
V4 (macaque)	Unattended (A) versus attended (B) (spatial + contrast discrimination)	333 ms	(0.85,1.05)*	134
V4 (macaque)	Attended with PFC lesion (A) versus attended (B)	150 ms	0.75	135
V1 (macaque)	Spontaneous (A) versus evoked (B) activity	100 ms	0.63	48
V1 (macaque)	Non-adapted (A) versus adapted (A) responses	1.86 s	0.78†	136
V1 (macaque)	Spontaneous (A) versus stimulation of the non-classical surround (B)	600 ms	0.85	137
V1 (macaque)	Anesthetized (A) versus awake (B)	500 ms	0.14	10
V1 (macaque)	Attended with drug application‡ (A) versus attended without drug (B)	300 ms	0.60, 0.4, 1.8	138
V1 (mouse)	Low (A) versus high (B) arousal	2 s, 150 ms	−0.22, 0.8	139,140
V1 (mouse)	Stationary (A) versus locomotion (B)	100 ms	0.45	141
A1 (macaque)	Passive (A) versus detection task (B)	Not given	0.5§	142
PFC (rhesus)	Untrained (A) versus trained (B)	100 ms	0.5	143
MSTd (macaque)	Untrained (A) versus trained (B)	100 ms	0.2‖	129
MT (rhesus)	Task cooperation (A) versus competition (B)	650 ms	(0.65,1.55)¶	144
Piriform cortex (mouse)	Pre-task (A) versus odor sniff (B)	120 ms	0.12	145
CLM (European starling)	untrained (A) versus task-relevant (B)	565 ms	(0.35, 1.65)#	146
Area 17 (cat)	Perpendicular (A) versus aligned (B) surround grating	1 ms	0.8**	147
V1 (cat)	Flashed stimuli (A) versus drifting grating (B)	100 ms	0.5	45
Intracellularly recorded membrane potentials				
V1 (cat)	Spontaneous (A) versus evoked (B) activity	0–10 Hz††	0.75	148
Barrel cortex (mouse)	Quiet wakefulness (A) versus active whisking (B)	2 ms	0.5	149
V1 (macaque)	Spontaneous (A) versus evoked (B) activity	0.5–4 Hz§§	0.5	150

We denote the two states with A and B, and the correlations measured in each state by ρ^A and ρ^B with $\rho^A > \rho^B$ unless otherwise noted. The reported ρ^A/ρ^B values are approximate.
*Neuron pairs were grouped according to their task tuning similarity (TTS). Neuron pairs with TTS > 1 show an attention-mediated decrease in ρ, whereas pairs with TTS < −1 show an increase. †Restricted to neuron pairs with $\rho^A > 0$. ‡Three different drugs were applied to recorded neurons during a cued spatial attention task: DL-2-amino-5-phosphonopentanoic acid (AP5), 6-cyano-7-nitroquinoxaline-2,3-dione (CNQX) and an NMDA receptor agonist; relative correlations are listed in that order. §Restricted to neurons with similar tuning. ‖Trained and untrained correlations are obtained from separate animals. ¶Task specifics placed neuron pairs to have either a cooperative relation to one another, or a competitive one. Neuron pairs were grouped according to the difference in their preferred direction of motion (PD), and competition decreased ρ for neuron pairs with PD < 135°, whereas it increased ρ for pairs with PD > 135°. #Neuron pairs with signal correlation > 0.4 show a relative modulation of 0.65, whereas pairs with a signal correlation < 0.4 show a modulation of −0.65. **Given that firing rate changes were negligible, the measures were computed only from $Cov(y_1, y_2)$. ††Computed from the integrated spectral coherence between simultaneously recorded membrane potentials. §§Computed from the integrated spectral coherence between simultaneously recorded membrane potential and nearby local field potential.

although it could still provide qualitative insights. For large time windows, T, the response function L/T is approximately the derivative (slope) of the firing rate versus input curve of a neuron at the operational point[37,38].

We assume that the response of each neuron is the result of a leaky, potentially nonlinear integration of its inputs. The total integrated input, $\hat{x}_i(t)$, includes presynaptic and postsynaptic components. The covariance between presynaptic inputs, $Cov(P_1, P_2)$, is determined by both common projections to the neuron pair, as well as correlations in the activity of the presynaptic pool of neurons[31,32]. From the vantage point of a postsynaptic neuron pair, these sources are indistinguishable. If we neglect synaptic and dendritic nonlinearities, then $Cov(\hat{x}_1, \hat{x}_2) \propto Cov(P_1, P_2)$, where the covariance on the right is between the activities, P_i^k, of the population presynaptic to neuron i (**Fig. 1**).

Postsynaptic effects, such as stochastic vesicle release from synaptic contacts or channel fluctuations, are another source of variability[52,53]. Given that these fluctuations are private to each neuron, we assume that they are uncorrelated between the neuron pair. Furthermore, they are also likely uncorrelated with the activity of the presynaptic population, so that $Var(\hat{x}_i) \propto Var(P_i) + Var(N_i)$, where N_i is the postsynaptic noise (integrated over T) in neuron i (**Fig. 1**). The total correlation coefficient of the inputs is then

$$\rho_x = \frac{Cov(\hat{x}_1, \hat{x}2)}{Var(\hat{x})} = \frac{Cov(P_1, P_2)}{Var(P) + Var(N)} = \frac{\rho_P}{1 + R_x}$$

where $R_x = Var(N)/Var(P)$ and $\rho_P = Cov(P_1, P_2)/Var(P)$. We again assume that $Var(\hat{x}) = Var(\hat{x}_1) = Var(\hat{x}_2)$, and similarly for the other variances. The coefficient R_x then measures the excess fluctuations in the input current resulting from internal processes in each neuron. Ultimately, we are interested in the variability of the spiking output of a neuron, n_i. Unfortunately, there is no simple linear relationship between $Var(n_i)$ and $Var(\hat{x}_i)$[54]. However, we make the reasonable assumption that there is a monotonic relationship between R_y and R_x, and hereafter make no distinction between R_x and R_y.

Finally, we consider the network to be in one of two states (labeled A and B) that differ in their correlation coefficient ρ. This analysis then yields the following expression for the ratio of ρ in the two states, A and B

$$\frac{\rho^B}{\rho^A} = \left(\frac{\rho_P^B}{\rho_P^A}\right)\left(\frac{1 + R^B}{1 + R^A}\right)^{-1}\left(\frac{L^B}{L^A}\right)^2 \qquad (2)$$

The modulation in ρ between the two states results from three separate terms. First, ρ_P^B/ρ_P^A captures state-dependent changes in the correlations of the presynaptic input. Second, $\left[(1+R)^B/(1+R)^A\right]^{-1}$ captures state-dependent changes in the internal fluctuations in each neuron in the pair. Third, $[L^B/L^A]^2$ captures state-dependent changes in the response gain of the transfer from synaptic input to the neurons' output. Generally $L^A \neq L^B$, as the linearization about the operational point at state A will typically differ from that at state B.

Figure 1 Schematic illustration of correlation transfer in networks of spiking neurons. We consider a pair of unconnected neurons (black triangles) that receive input from a presynaptic population of excitatory neurons (red triangles) and inhibitory neurons (blue circles). Covariability, $Cov(P_1, P_2)$, in the presynaptic inputs, P_1 and P_2, to the postsynaptic pair is a result of a combination of shared anatomical projections leading to a shared input (overlap between P_1 and P_2) and correlations between the activity of the presynaptic populations. This presynaptic activity along with internal synaptic and cellular fluctuations, N_i, determine the postsynaptic currents, x_i ($i = 1, 2$), in each of the two postsynaptic cells. Finally, the nonlinear spike generation mechanism translates these postsynaptic currents into the output spike trains, y_1 and y_2.
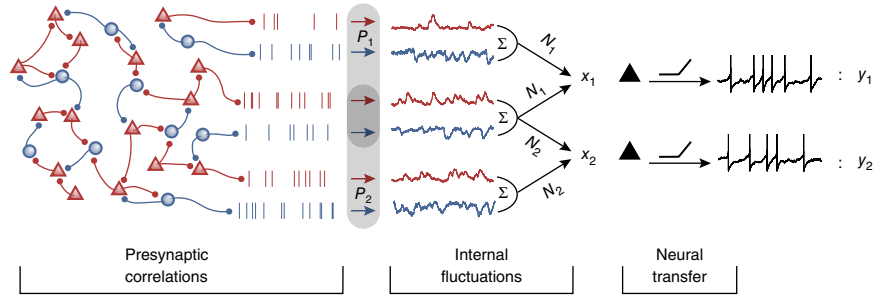
We next explore each of these modulatory terms in our feedforward network.

Three mechanisms of correlation modulation

There are several distinct ways to model a state change in a network. For example, neuromodulation through cholinergic and monoaminergic pathways can have diverse effects on the cellular and synaptic properties in a network[55]. Alternatively, the dynamics of large-scale neural activity, as measured by electroencephalogram (EEG) and local field potential (LFP) recordings, differ between two neural states[41]. This can be modeled by changing the statistics of a global input to the network[9–11,56].

In our framework, a presynaptic pool of excitatory and inhibitory neurons project to a representative neuron pair (**Fig. 2**). We model the shift from state A to state B as an increase in a static external drive to the presynaptic neuron population (**Fig. 2a,b,e,f,j**). This modeling choice causes changes in both the firing rate and correlations of the postsynaptic pair and can be loosely interpreted as capturing a wide array of neuromodulation schemes. We examine this general model of modulation (see **Supplementary Mathematical Note** for a description of the model) in three examples, each highlighting a different mechanism of correlation modulation.

Modulating presynaptic correlations

We start by analyzing the effect of changes in the correlations in the pool of presynaptic neurons. Here, as in other examples, the target pair of neurons receive correlated excitatory (E) and correlated inhibitory (I) inputs via an overlapping set of projections from the presynaptic pool. In the present case we also include direct connections from excitatory to inhibitory neurons within the presynaptic pool itself. These connections can correlate the inhibitory activity received by one neuron in the pair with the excitatory activity received by the other neuron. The covariance of the total presynaptic activity, $P_i = \hat{E}_i + \hat{I}_i$, is computed as

$$Cov(P_1, P_2) = Cov(\hat{E}_1, \hat{E}_2) + Cov(\hat{I}_1, \hat{I}_2) + Cov(\hat{E}_1, \hat{I}_2) + Cov(\hat{I}_1, \hat{E}_2) \quad (3)$$

In state A, both excitatory and inhibitory presynaptic pools are weakly driven, resulting in low firing rates in the presynaptic populations and subsequently low firing rates of the postsynaptic neuron pair. The low rates in the presynaptic populations allow the spike threshold nonlinearity of the presynaptic cells to suppress neural transfer (the response gain L of the presynaptic populations is small). This compromises the presynaptic inhibitory pool's response to projections from the excitatory presynaptic population. In particular, the low firing rates in the inhibitory pool imply that the inhibitory pool transfers poorly the excitatory input fluctuations to the postsynaptic neuron pair. This results in approximately uncorrelated outputs of the excitatory and inhibitory pool, $Cov(\hat{E}_i, \hat{I}_j) \approx 0$ (**Fig. 2c**). In this case, ρ^A is primarily a result of overlapping projections with $Cov(\hat{E}_1, \hat{E}_2) > 0$ and $Cov(\hat{I}_1, \hat{I}_2) > 0$.

In state B, the presynaptic pool of neurons fires at a higher rate, increasing the net input to the postsynaptic pair, yielding a higher postsynaptic firing rate compared to state A (**Fig. 2d**). Furthermore, given that the drive to the inhibitory pool in state B is larger than in state A, the spiking nonlinearity of the inhibitory neurons does not compromise their response to the projections from the excitatory pool. Thus, the activity of the presynaptic inhibition is correlated with that of the presynaptic excitation. However, given that inhibition is hyperpolarizing, whereas excitation is depolarizing, the projections from the excitatory pool to one postsynaptic neuron are anticorrelated with the inhibitory projections to the other postsynaptic neuron. In the end, $Cov(\hat{E}_i, \hat{I}_j) < 0$ (**Fig. 2c**), and this negative covariability partially cancels the positive covariability due to overlapping projections. This has the effect of reducing overall input correlations, so that $\rho_P^B / \rho_P^A < 1$. This leads to a reduction in output correlations (**Fig. 2d**) with $\rho^B / \rho^A < 1$ (via equation (2)). In this example, the linear transfer function remained approximately constant between the two states ($L^A \approx L^B$) and we did not model private fluctuations ($R^A = R^B = 0$).

Excitatory and inhibitory currents are widely reported to be strongly correlated with one another[57–59]. In our model, such correlations are a result of feedforward excitatory and the associated disynaptic inhibitory pathways, a canonical circuit in the brain[60]. The functional consequences of this type of connectivity were first investigated from trial-averaged single neuron activity, with delayed inhibition creating a 'window of opportunity' for neural responses[21,61–63]. Recent studies have investigated the influence of this circuit structure on correlations between excitation and inhibition and the covariability of population responses. In the whisker barrel cortex of rodents, this circuit structure supports an active decorrelation of the spiking activity between excitatory and inhibitory neurons when measured in the stimulus evoked state[64,65]. A functionally similar feedforward circuit in the electrosensory system of weakly electric fish drives a decorrelated state when stimuli are spatially broad as opposed to spatially compact[66,67]. The example presented above is based on the models developed in those studies.

Renart, de la Rocha and colleagues initially studied the cancelation of overall input current covariability by anti-correlated excitatory and inhibitory inputs to neuron pairs[32]. However, they considered the case of recurrently coupled cortical networks, as opposed to the feedforward structure analyzed above. They showed that, in balanced networks of neurons[68], the large sources of correlation resulting from shared

Figure 2 Three mechanisms for correlation modulation. (**a**) The presynaptic excitatory (E) population (red) and the inhibitory population (blue) both project to the postsynaptic neuron pair. In state A the presynaptic populations are weakly driven, with a slight asymmetry favoring the E population. (**b**) In contrast, both presynaptic E and I populations are driven strongly in state B. (**c**) The increase in presynaptic rate uncovers an anticorrelation between the E and I currents, ultimately decorrelating the overall synaptic inputs to the postsynaptic pair. (**d**) The result of the modulation from state A to B is to both increase the postsynaptic firing rate (green) and decrease spike count correlation (black). (**e**) The synapses linking presynaptic activity to postsynaptic current are probabilistic, with activity-dependent reliability of vesicle release (we show only the E population for schematic brevity). In state A, the presynaptic populations are weakly driven and the number of vesicles released per presynaptic spike, and their reliability, is high. (**f**) In contrast, in state B, the presynaptic population fires at a higher rate, resulting in less reliable synaptic transmission. (**g**) The decrease in synaptic reliability from state A to B increases the synaptic noise-to-signal ratio,

1 + R. (**h**) The transition from state A to B has the effect of both increasing the postsynaptic firing rate (green) and decreasing the spike count correlation (black). (**i**) The presynaptic E and I populations project balanced, conductance based inputs to the postsynaptic pair. In state A, the firing rates of the presynaptic populations are low, and the overall synaptic fluctuations are small. (**j**) In contrast, in state B the presynaptic rates are higher, resulting in larger fluctuations in the input to the postsynaptic pair. (**k**) The increase in conductance-based fluctuations between state A and B reduces the spike response gain (L). (**l**) The transition from state A to B increases the postsynaptic firing rate (green) and decreases the spike count correlation (black).
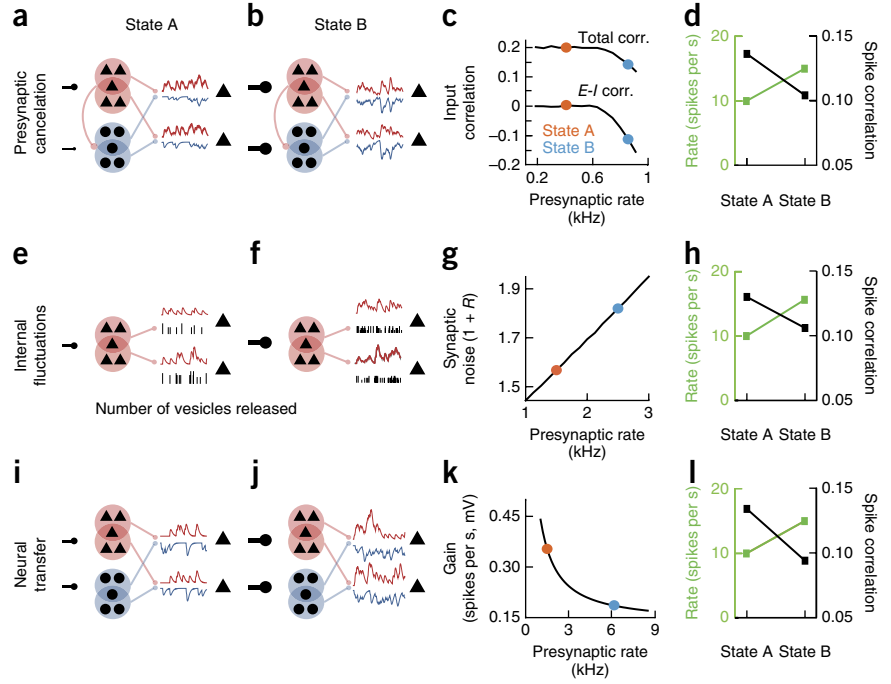
projections in and outside the circuit were robustly and fully cancelled, stabilizing an asynchronous network state. Conditions under which such cancellation occurs have been clarified in further studies of recurrently coupled networks of model spiking neurons[69,70]. Modulation of correlations is difficult to study in these cases, mainly because correlations are very small (on the order of the inverse of the network size). We will revisit correlation modulation in recurrent networks later.

In sum, the circuit mechanisms that determine presynaptic covariability are diverse, and a complete treatment is beyond the scope of this review. Nevertheless, in many cases a cancellation between various sources of opposing pre-synaptic correlations is a key component.

Modulating postsynaptic noise

To demonstrate the influence of private noise on correlation transfer, we consider a model in which synaptic release is random. Every presynaptic spike releases a random number of synaptic vesicles to the postsynaptic neuron[53]. This is a result of both the nature of vesicle release and the fact that vesicles are replenished at random times. Vesicle recovery dynamics result in activity-dependent changes in the synaptic current's mean and variability. This type of synaptic dynamics is standard in models of short-term synaptic depression and has been widely used in past studies[71–75].

We again consider the response of our model neuron pair in two states. In state A, the modulatory drive is weak and presynaptic populations fire at a low rate. In this case, the variability in the postsynaptic current, $Var(N)$, is primarily a result of probabilistic vesicle release, as vesicle uptake almost always happens before the next spike arrival. Thus the relative synaptic noise, $R^A = Var(N^A)/Var(P^A)$, is small (**Fig. 2g**). As a result, the output correlation, ρ^A, is only weakly diluted by synaptic noise.

In contrast, the larger modulatory drive in state B results in higher presynaptic and postsynaptic firing rates (**Fig. 2h**). Higher postsynaptic

activity results in increased depression of synaptic transfer as a result of vesicle depletion. The probabilistic nature of vesicle recovery increases fluctuations in the synaptic current, so that relative synaptic noise, R^B, is larger than in state A (**Fig. 2g**). Given that vesicle recovery is independent across synapses, such increased variability dilutes input correlations, ρ^B. This results in a modulation of output spiking correlations with $\rho^B < \rho^A$ (**Fig. 2h**).

Variability resulting from internal release and recovery dynamics in individual synapses is well documented[53,76]. Previous studies focused on the effect of such synaptic variability on the information transmission across a synapse[75,77]. Here we follow our past study[78] and show how input correlations are diluted by synaptic variability in a firing rate dependent manner (also see ref. 79).

Synaptic variability is not the only cause of correlation dilution. Alternative mechanisms only need two features. First, the variability must be independent across neurons, so that $Cov(\hat{x}_1, \hat{x}_2)$ is unaffected by changes in state. Second, the variability must be activity dependent so that R changes with the state[80,81]. A multitude of biophysical mechanisms satisfy these requirements, including fast membrane potential fluctuations resulting from stochastic openings and closings of ion channels[52,81], action potential threshold fluctuations resulting from finite-sized populations of axonal sodium channels[82], and slow fluctuations in the cellular excitability of neurons[83].

Modulating neural transfer

In the previous examples, the intensity of background synaptic fluctuations changed the input statistics. We next show how it can also influence output correlations by changing the response gain (L) of a neuron. In our example, the drive from the presynaptic populations is balanced, meaning that both excitation and inhibition increase with the modulatory input (**Fig. 2i,j**). We chose parameters so that the total mean presynaptic input to the target pair is approximately

Figure 3 Dissecting correlation modulation. (**a**–**c**) Output correlation coefficient ρ as a function of the window T over which spike trains are counted. The presynaptic correlations (column 1), internal fluctuation (column 2) and neural transfer (column 3) examples are identical to those of **Figure 2**. (**d**–**f**) The Fano factor, $F(n) = Var(n)/<n>$, for the data shown in **a**–**c**. (**g**–**i**) The co-Fano factor, $CoF(n_1, n_2) = Cov(n_1, n_2)/<n>$, for the data shown in **a**–**c**.

state independent (through a cancelation of excitation and inhibition currents), but the overall variability of the synaptic input increases with the modulatory drive so that $Var(P^B) > Var(P^A)$. Furthermore, the modulation is such that despite the increase in variance the presynaptic correlations remained fixed, that is $\rho_P^B = \rho_P^A$. Finally, we neglect synaptic variability, so that $R^A = R^B = 0$. Thus, any change in output correlation, ρ, cannot be due to a change in input correlation, ρ_x.

Modeling work[84–87], dynamic-clamp slice experiments[88,89] and *in vivo* whole-cell recording[90] have all demonstrated that increases in conductance-based input fluctuations lower L. Indeed, in our model, given that synaptic fluctuations are larger in state B than in state A, it follows that $L^B < L^A$ (**Fig. 2k**). Thus, despite the increase in firing rate between state A and B (**Fig. 2l**), and the absence of changes in the input correlations, $\rho^A = \rho^B$, we nevertheless observe $\rho^B < \rho^A$ (**Fig. 2l**). The reduction of L by increased synaptic activity is well studied[88], and the subsequent decrease in output correlations under this modulation scheme has been previously noted[89].

Calculating the response gain, L, and determining its effect on the collective behavior of neuronal populations has a long history[50,51,91]. In particular, the example of a pair of uncoupled neurons driven by partially correlated inputs has been extensively studied. Formally, the nonlinear transfer between continuous input and spike response ensures that $\rho < \rho_x$[37,39,92–94], yet the influence of the nonlinearity can be controlled by several factors. In many neuron models, L increases with the firing rate of a neuron, resulting in a relationship between firing rates and ρ[37,38,95]. This prediction has been verified in a variety of experimental studies[10,25,95,96], and firing rate is often a core determinant of output correlation[45]. However, in general, output spiking correlations and firing rate do not have a prescribed relation, as our examples illustrate (**Fig. 2d,h,l**).

Neural excitability can shape how input correlations are transferred to output correlations, with neural integrators favoring spike count correlations measured over long timescales[93], whereas resonator and phasic membrane dynamics show enhanced short timescale synchrony[97–100]. Subthreshold cellular dynamics, such as spike-frequency adaptation[101] or fast membrane tracking of slow synaptic inputs[92], also shape L and hence the transfer of correlation. Increased cellular heterogeneity between the postsynaptic neuron pair typically reduces ρ[38,102], particularly when measured over short timescales[38,103,104]. These studies all explicitly considered the case of correlation transfer for a neuron pair; however, the cellular and synaptic mechanisms that determine the response gain of a neuron have been a long-standing topic of interest[105]. Our theory suggests that all of these gain control mechanisms will also influence correlation transfer.

Distinguishing between the mechanisms

These three examples demonstrate how distinct physiological mechanisms impact both firing rates and pairwise correlations. We have chosen model parameters so that the changes in firing rate and correlations are nearly identical in all three cases (**Fig. 2d,h,l**). This illustrates an inherent difficulty in using changes in output statistics to infer the biophysical mechanisms that have caused them.

One way to distinguish the mechanisms underlying correlation modulation is to consider spiking correlations ρ as a function of the time window (T) over which they are computed, as different mechanism modulate
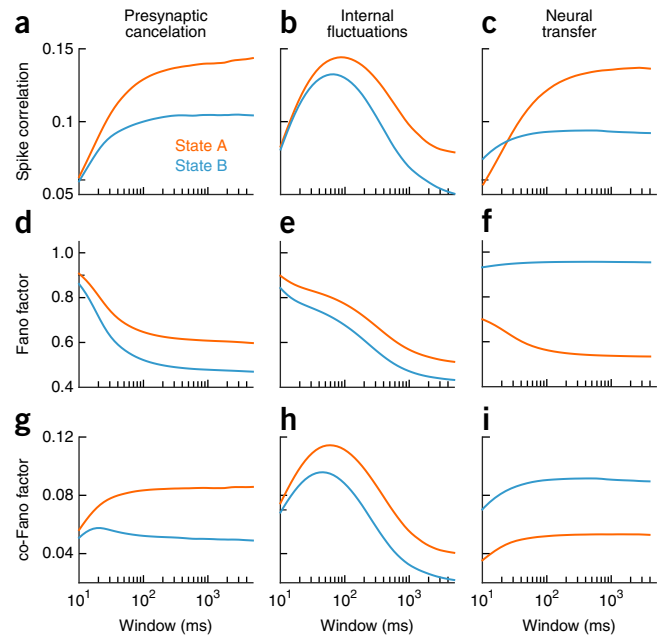
correlations on different timescales[78,89,101]. In general, ρ increases with the time window[106], as in the case of the feedforward model with non-plastic synapses (**Fig. 3a,c**). However, synapses with short-term depression have long timescale vesicle uptake dynamics (~ 400 ms), attenuating low frequency pre- to postsynaptic transfer. Consequently, broadband presynaptic activity is not correlated with postsynaptic responses over long timescales, and thus ρ is reduced for $T > 400$ s (**Fig. 3b**). Although measuring ρ as a function of T can help to distinguish some mechanisms from others, it does not provide a perfect diagnostic. Indeed, some qualitatively distinct mechanisms may only show quantitative differences in the timescale dependence of ρ (**Fig. 3a,c**).

Another way to distinguish the mechanisms is to recall that ρ is defined as a ratio

$$\rho = \frac{Cov(n_1, n_2)}{Var(n)} = \frac{CoF(n_1, n_2)}{F(n)}$$

In the second equality we used the co-Fano factor[93], $CoF(n_1, n_2) = Cov(n_1, n_2)/\langle n \rangle$, and the Fano factor, $F(n) = Var(n)/\langle n \rangle$ ($\langle n \rangle$ is the mean spike count). A decrease in ρ between state A and B may be a result of either a larger decrease in $CoF(n_1, n_2)$ than $F(n)$ or a larger increase in $F(n)$ than $CoF(n_1, n_2)$. The cancelation of presynaptic covariability through feedforward inhibition or an increase in variability through probabilistic vesicle release both lead to a reduction in ρ, as in the first case (**Fig. 3d,e,g,h**). In contrast, larger overall variability with increased background fluctuations coupled with a reduced gain leads to a reduction in ρ, as in the second case (**Fig. 3f,i**). However, as with timescales, separating modulations of ρ into modulations of spike count Fano and co-Fano factors can only give partial information about underlying biophysical mechanisms.

It is possible to indirectly measure the stimulus-response gain L of a neuron by ranging over a stimulus parameter. If the stimulus dependence and the sources of input variability are known (or can be approximated) then one can account for changes in ρ by changes in L[66]. Manipulations of a neural circuit by pharmacological or optogenetic means can give further insights into how the organization of presynaptic correlations, ρ_p, or postsynaptic variability, R, contributes to state-dependent changes in ρ (see below).

The most direct method to characterize the mechanisms responsible for state-dependent changes in correlation remains to use whole-cell recordings of membrane potential voltage fluctuations. Whole-cell recordings give information about both the synaptic inputs and spike outputs, allowing us to measure input correlations, $Cov(x_1, x_2)$, internal fluctuations, R, and response gain, L, directly. Although *in vivo* whole-cell recording is challenging, there are several studies where pairwise correlations have been modulated and simultaneous membrane potentials, or a membrane potential and local field potential have been recorded (**Table 1**). Studies of this type continue to be well suited to uncover the physiological basis of state-dependent correlation modulation.

Correlation modulation in recurrent networks

Thus far, we have explored correlation modulation in a simple feedforward circuit (**Figs. 1** and **2**). However, a primary characteristic of cortical networks is recurrent connectivity between neurons. Several groups have analyzed various models of recurrent networks of excitatory and inhibitory neurons[107–109], and have provided key insights into the mechanisms that shape spike train correlations. For instance, networks with rapid, but delayed, recurrent inhibition produce fast-timescale correlated activity in the γ frequency range (30–70 Hz)[50,110,111], but often show negligible correlations on slow timescales. Networks with weak or balanced coupling produce slow-timescale correlated activity whose magnitude scales inversely with system size, becoming exceedingly small in networks with thousands of neurons[32,34,35,69,112]. However, we are far from a complete understanding of self-generated correlated activity in recurrently networks of spiking neurons.

Clustered feedforward[113], clustered recurrent[114–116] and spatially distributed network architectures[47,117,118] can all produce correlated activity between spiking neurons. In such networks, only neurons that belong to the same cluster or are close to one another are strongly correlated. Indeed, experiments show that noise correlations are large for neuron pairs that are reciprocally connected[119] (same putative cluster), similarly tuned or are nearby in space to one another[48]. However, the correlation between neuron pairs that fall outside these categories are also, on average, positive[48].

Parallel recordings from neural populations show that network-wide correlations can be largely explained by a one dimensional source of shared fluctuations, often treated as a latent variable in statistical approaches[9–11,56,120]. The origin of this source is not known. A straightforward (albeit phenomenological) way to model these dynamics is to drive a network of spiking neurons with a spatially coherent input that represents an external source of fluctuations[28,56,94,121–123]. Using this strategy, we can study correlation modulation in recurrent networks.

We consider a network of model excitatory (E) and inhibitory (I) spiking neurons with dense, recurrent connections between them. Weak feedforward input fluctuations, $F(t)$, are shared by all neurons (providing feedforward covariability Cov_F), alongside private fluctuations specific to each neuron in the network (**Fig. 4a**). The shared fluctuations are the largest source of network covariability in the model. In addition, we assume that there is a modulatory input similar to that of our previous models (**Fig. 2**) that depolarizes all neurons (different magnitude for E and I neurons). This modulatory input does not affect the external fluctuations $F(t)$.

In response to the modulation, E neurons have a higher firing rate in state B than state A (**Fig. 4b,e**). In both states, the shared fluctuations produce substantial variability in the instantaneous population firing rates (**Fig. 4b**). If the strength of shared input fluctuations is small compared with private fluctuations, then the linear response

framework assumed in equation (2) is valid[28,66,112,121,122,124]. In this case, the intuition developed from our feedforward analysis will apply to a representative pair of neurons selected from the network. However, to understand the modulation of neural correlations, ρ, we must understand the combined modulations of the presynaptic input correlations, the transfer of presynaptic activity to synaptic current x and the gain of the postsynaptic response to those currents, L.

The nonlinearity of the transfer between synaptic input and spike response allows the gain L to be state dependent. In our model, we have that $L^A < L^B$ (**Fig. 4c**). This differs from our previous analysis (**Fig. 2k**), as the network model has current-based synapses, whereas the feedforward case has conductance-based synapses, mimicking a high-conductance state[89]. With current-based synapses and moderate firing rates, an increase in firing rate results in an increase in L, which is supported both by *in vitro*[37,105] and *in vivo*[20] recordings. Thus, in our model, it is expected that the modulation will produce $L^B/L^A > 1$.

Any pair of neurons in our network is correlated through the shared fluctuations $F(t)$ via two pathways: the direct feedforward component that provides input with covariance Cov_F between neurons, and the indirect pathway via recurrent excitatory and inhibitory projections between neurons in the network that also receive $F(t)$. To simplify the exposition, we consider the joint common recurrent input $R(t) = E(t) + I(t)$. The full covariance of the presynaptic input to a neuron pair then decomposes as

$$Cov(P_1, P_2) = Cov_F + Cov_R + 2Cov_{FR}$$

Here Cov_R is the covariability resulting from common recurrent input to the neuron pair, whereas Cov_{FR} is the interaction between the feedforward and recurrent pathways. This decomposition is similar to feedforward case shown in equation (3). Although the feedforward input $F(t)$ is state invariant, the recurrent activity $R(t)$ changes with state. In our model, the inhibitory pathway is dominant, making $Cov_{FR} < 0$ because dynamic recurrent inhibition acts to partially cancel the feedforward drive[69,121]. The modulatory input enhances this cancellation so that $Cov_R^A + 2Cov_{FR}^A > Cov_R^B + 2Cov_{FR}^B$, ultimately yielding $Cov^A(P_1, P_2) > Cov^B(P_1, P_2)$ (**Fig. 4d**).

The combined effect of the modulation is to produce two opposing manipulations of correlation transfer. An increase in response gain ($L^B/L^A > 1$) occurs in tandem with a decorrelation of the presynaptic input ($Cov(P_1, P_2)^B / Cov(P_1, P_2)^A < 1$). Our theory in equation (2) suggests that the response gain modulation will produce an increase in correlation in state B, that is $\rho^B/\rho^A > 1$, whereas the presynaptic correlation modulation leads to decrease, $\rho^B/\rho^A < 1$. We chose a modulation so that the latter effect dominates, and the spike correlation is reduced in state B (**Fig. 4e**). In general, modulatory inputs result in state changes in multiple stages of correlation transfer.

As in the feedforward networks, it is difficult to use spike train data alone to dissect the individual contributions of gain and presynaptic correlation modulations in a recurrent network. Further probing of the network can, however, give insight into the mechanisms of correlation modulation. To illustrate, we model an experiment in which light is used to activate interneurons expressing halorhodopsin in a cortical network (**Fig. 4f**). We assume that light hyperpolarizes a fraction (50%) of the I cells in our model. Removing a large fraction of recurrent inhibition changes state-dependent modulations in two important ways. First, the increase in firing rates in going from state A to B is much larger (**Fig. 4g**). Second, spike correlations now increase with the state modulation (**Fig. 4f**).

With weaker inhibition, the cancellation of feedforward correlations Cov_F through Cov_{FR} is attenuated. Thus, when halorhodopsin is

Figure 4 Correlation modulation in recurrent networks. (**a**) Schematic of recurrent excitatory (*E*) and inhibitory (*I*) network. The neurons in the network receive a global source of shared fluctuations, alongside individual sources of private variability. (**b**) Spike train rasters (top) and instantaneous firing rates (bottom) of a subset of the *E* neuron population in state A and B. (**c**) Change in spike response gain (*L*) as modulatory drive (state) is varied. (**d**) Change in presynaptic correlation to a representative pair of neurons in the population as modulatory drive (state) is varied. (**e**) The result of the modulation from state A to B is to both increase the postsynaptic firing rate (green) and decrease spike count correlation (black). (**f**) Schematic showing a silencing of a portion of the inhibitory population through activation of halorhodopsin. (**g**) Results are presented as in **e**, but with half of the inhibitory neurons hyperpolarized.
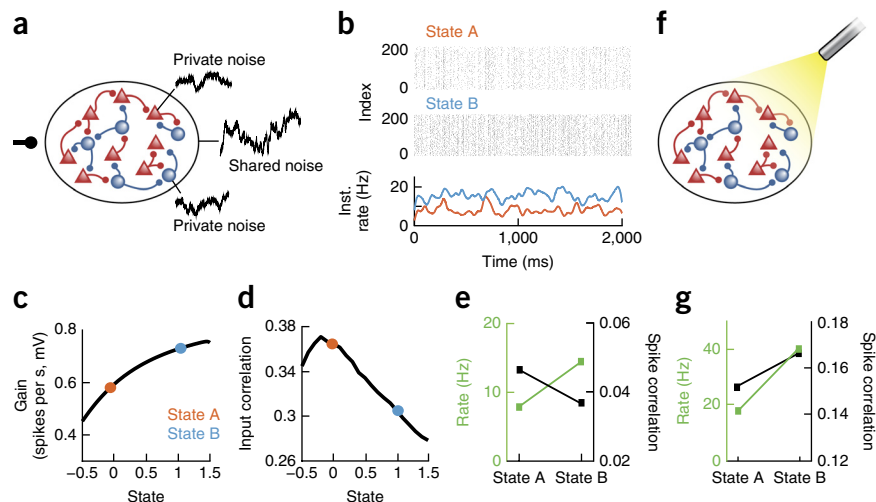
activated, the decorrelation in neural activity through recurrent inhibition is compromised. Furthermore, the increase in firing rate with decreased inhibition allows *L* to increase to a larger extent as the network transitions from state A to B. The combination of these effects leads to an increase in ρ with the state change when inhibition is reduced. Had recurrent inhibition not been a primary component of the mechanism underlying the state-dependent modulation in the control case, then we would not expect to observe these qualitative changes.

This example shows how contemporary circuit manipulation techniques can be used to test concrete predictions about state-dependent correlation changes in recurrent networks. We have confined our analysis to networks with weak coupling that receive external sources of fluctuations[34,35,66,69,121,122]. In this case, linear response techniques are valid. The network simply transforms global input fluctuations into network-wide spiking correlations. However, when coupling is stronger the network can generate globally coherent activity[50,110,111] and strong[125] or slow[115,126] fluctuations. The complete analysis of such dynamics involves the nonlinear network properties, and hence the factorization in equation (2) is not applicable. Such behavior is beyond the scope of this review.

Conclusion

Here we present a general framework for analyzing the physiological mechanisms underlying the modulations of neuronal correlations. We demonstrate our theory using several examples; however, the list of mechanisms that we considered was not exhaustive. The large number of factors that modulate intrinsic cellular properties, as well as synaptic excitation and inhibition, suggest that many distinct mechanisms control neuronal correlation. Our theoretical approach allows for an easier navigation of this large space, and the development of a mechanistic understanding of state-dependent modulation of neuronal activity.

Unraveling the mechanics of correlation modulation *in vivo* will require a concerted experimental effort. We noted that whole-cell recordings will give invaluable data to validate the aspects of certain mechanisms over alternative ones. In addition, the combination of genetic specification[127] and targeted optogentic manipulation of neural circuits[128] promises to provide some fundamental insights. Finally, analysis of population-wide recordings describes how pair-wise correlations are distributed across large groups of neurons[9–11,56,120]. Extending our theory to networks of neurons is straightforward[34,121,122]. However, understanding how

the dimensionality of population wide input correlation is represented by the spike responses of interconnected neurons is an open challenge.

The changes in correlated activity that we describe may have a number of consequences for neural coding. Theoretical[26,123] and experimental[96,129,130] studies have shown that changes in correlations can increase the accuracy with which stimulus can be decoded from the population response. Furthermore, increased synchrony has also been shown to precede behaviorally relevant events[131]. However, recent work has exposed that it is the degree of overlap between the structure of population noise correlations and population stimulus tuning that ultimately identifies the correlations that limit information transfer[28]. This implies that conclusions about the effect of noise correlations on neural coding should be made with care.

We have come a long way in characterizing the mechanics underlying the responses of single neurons. Understanding circuit and cellular modulations of the collective activity of neural populations will be an essential step toward understanding the brain.

A **Supplementary Methods Checklist** is available.

Note: Any Supplementary Information and Source Data files are available in the online version of the paper.

1. Ganmor, E., Segev, R. & Schneidman, E. A thesaurus for a neural population code. *eLife* **4**, e06134 (2015).
2. Buzsáki, G. Neural syntax: cell assemblies, synapsembles, and readers. *Neuron* **68**, 362–385 (2010).
3. Beck, J.M. *et al*. Probabilistic population codes for Bayesian decision making. *Neuron* **60**, 1142–1152 (2008).
4. Rigotti, M. *et al*. The importance of mixed selectivity in complex cognitive tasks. *Nature* **497**, 585–590 (2013).
5. Yuste, R. From the neuron doctrine to neural networks. *Nat. Rev. Neurosci.* **16**, 487–497 (2015).

6. Sherman, S.M. & Guillery, R.W. On the actions that one nerve cell can have on another: distinguishing "drivers" from "modulators". *Proc. Natl. Acad. Sci. USA* **95**, 7121–7126 (1998).

7. Pillow, J.W. *et al.* Spatio-temporal correlations and visual signaling in a complete neuronal population. *Nature* **454**, 995–999 (2008).

8. Cunningham, J.P. & Yu, B.M. Dimensionality reduction for large-scale neural recordings. *Nat. Neurosci.* **17**, 1500–1509 (2014).

9. Goris, R.L., Movshon, J.A. & Simoncelli, E.P. Partitioning neuronal variability. *Nat. Neurosci.* **17**, 858–865 (2014).

10. Ecker, A.S. *et al.* State dependence of noise correlations in macaque primary visual cortex. *Neuron* **82**, 235–248 (2014).

11. Lin, I.C., Okun, M., Carandini, M. & Harris, K.D. The Nature of shared cortical variability. *Neuron* **87**, 644–656 (2015).

12. Ledoit, O. & Wolf, M. A well-conditioned estimator for large-dimensional covariance matrices. *J. Multivariate Anal.* **88**, 365–411 (2004).

13. Yatsenko, D. *et al.* Improved estimation and interpretation of correlations in neural circuits. *PLoS Comput. Biol.* **11**, e1004083 (2015).

14. Stevenson, I.H. & Kording, K.P. How advances in neural recording affect data analysis. *Nat. Neurosci.* **14**, 139–142 (2011).

15. Hubel, D.H. & Wiesel, T.N. Receptive fields, binocular interaction and functional architecture in the cat's visual cortex. *J. Physiol. (Lond.)* **160**, 106–154 (1962).

16. Ferster, D. & Miller, K.D. Neural mechanisms of orientation selectivity in the visual cortex. *Annu. Rev. Neurosci.* **23**, 441–471 (2000).

17. Ben-Yishai, R., Bar-Or, R.L. & Sompolinsky, H. Theory of orientation tuning in visual cortex. *Proc. Natl. Acad. Sci. USA* **92**, 3844–3848 (1995).

18. Sompolinsky, H. & Shapley, R. New perspectives on the mechanisms for orientation selectivity. *Curr. Opin. Neurobiol.* **7**, 514–522 (1997).

19. Ringach, D.L., Hawken, M.J. & Shapley, R. Dynamics of orientation tuning in macaque primary visual cortex. *Nature* **387**, 281–284 (1997).

20. Priebe, N.J. & Ferster, D. Inhibition, spike threshold, and stimulus selectivity in primary visual cortex. *Neuron* **57**, 482–497 (2008).

21. Bruno, R.M. & Simons, D.J. Feedforward mechanisms of excitatory and inhibitory cortical receptive fields. *J. Neurosci.* **22**, 10966–10975 (2002).

22. Liu, B.H., Wu, G.K., Arbuckle, R., Tao, H.W. & Zhang, L.I. Defining cortical frequency tuning with recurrent excitatory circuitry. *Nat. Neurosci.* **10**, 1594–1600 (2007).

23. Barak, O. & Tsodyks, M. Working models of working memory. *Curr. Opin. Neurobiol.* **25**, 20–24 (2014).

24. Giocomo, L.M., Moser, M.B. & Moser, E.I. Computational models of grid cells. *Neuron* **71**, 589–603 (2011).

25. Cohen, M.R. & Kohn, A. Measuring and interpreting neuronal correlations. *Nat. Neurosci.* **14**, 811–819 (2011).

26. Averbeck, B.B., Latham, P.E. & Pouget, A. Neural correlations, population coding and computation. *Nat. Rev. Neurosci.* **7**, 358–366 (2006).

27. Ecker, A.S., Berens, P., Tolias, A.S. & Bethge, M. The effect of noise correlations in populations of diversely tuned neurons. *J. Neurosci.* **31**, 14272–14283 (2011).

28. Moreno-Bote, R. *et al.* Information-limiting correlations. *Nat. Neurosci.* **17**, 1410–1417 (2014).

29. Hu, Y., Zylberberg, J. & Shea-Brown, E. The sign rule and beyond: boundary effects, flexibility and noise correlations in neural population codes. *PLoS Comput. Biol.* **10**, e1003469 (2014).

30. Shadlen, M.N. & Newsome, W.T. The variable discharge of cortical neurons: implications for connectivity, computation, and information coding. *J. Neurosci.* **18**, 3870–3896 (1998).

31. Rosenbaum, R., Trousdale, J. & Josić, K. The effects of pooling on spike train correlations. *Front. Neurosci.* **5**, 58 (2011).

32. Renart, A. *et al.* The asynchronous state in cortical circuits. *Science* **327**, 587–590 (2010).

33. Pernice, V., Staude, B., Cardanobile, S. & Rotter, S. How structure determines correlations in neuronal networks. *PLoS Comput. Biol.* **7**, e1002059 (2011).

34. Trousdale, J., Hu, Y., Shea-Brown, E. & Josić, K. Impact of network structure and cellular response on spike time correlations. *PLoS Comput. Biol.* **8**, e1002408 (2012).

35. Helias, M., Tetzlaff, T. & Diesmann, M. The correlation structure of local neuronal networks intrinsically results from recurrent dynamics. *PLoS Comput. Biol.* **10**, e1003428 (2014).

36. Wimmer, K. *et al.* Sensory integration dynamics in a hierarchical network explains choice probabilities in cortical area MT. *Nat. Commun.* **6**, 6177 (2015).

37. de la Rocha, J., Doiron, B., Shea-Brown, E., Josić, K. & Reyes, A. Correlation between neural spike trains increases with firing rate. *Nature* **448**, 802–806 (2007).

38. Shea-Brown, E., Josić, K., de la Rocha, J. & Doiron, B. Correlation and synchrony transfer in integrate-and-fire neurons: basic properties and consequences for coding. *Phys. Rev. Lett.* **100**, 108102 (2008).

39. Tchumatchenko, T., Malyshev, A., Geisel, T., Volgushev, M. & Wolf, F. Correlations and synchrony in threshold neuron models. *Phys. Rev. Lett.* **104**, 058102 (2010).

40. Churchland, M.M. *et al.* Stimulus onset quenches neural variability: a widespread cortical phenomenon. *Nat. Neurosci.* **13**, 369–378 (2010).

41. Harris, K.D. & Thiele, A. Cortical state and attention. *Nat. Rev. Neurosci.* **12**, 509–523 (2011).

42. McGinley, M.J. *et al.* Waking state: rapid variations modulate neural and behavioral responses. *Neuron* **87**, 1143–1161 (2015).

43. Eggermann, E., Kremer, Y., Crochet, S. & Petersen, C.C. Cholinergic signals in mouse barrel cortex during active whisker sensing. *Cell Rep.* **9**, 1654–1660 (2014).

44. Bair, W., Zohary, E. & Newsome, W.T. Correlated firing in macaque visual area MT: time scales and relationship to behavior. *J. Neurosci.* **21**, 1676–1697 (2001).

45. Schulz, D.P.A., Sahani, M. & Carandini, M. Five key factors determining pairwise correlations in visual cortex. *J. Neurophysiol.* **114**, 1022–1033 (2015).

46. Ecker, A.S. *et al.* Decorrelated neuronal firing in cortical microcircuits. *Science* **327**, 584–587 (2010).

47. Hansen, B.J., Chelaru, M.I. & Dragoi, V. Correlated variability in laminar cortical circuits. *Neuron* **76**, 590–602 (2012).

48. Smith, M.A. & Kohn, A. Spatial and temporal scales of neuronal correlation in primary visual cortex. *J. Neurosci.* **28**, 12591–12603 (2008).

49. Gururangan, S.S., Sadovsky, A.J. & MacLean, J.N. Analysis of graph invariants in functional neocortical circuitry reveals generalized features common to three areas of sensory cortex. *PLoS Comput. Biol.* **10**, e1003710 (2014).

50. Brunel, N. & Hakim, V. Fast global oscillations in networks of integrate-and-fire neurons with low firing rates. *Neural Comput.* **11**, 1621–1671 (1999).

51. Lindner, B. & Schimansky-Geier, L. Transmission of noise coded versus additive signals through a neuronal ensemble. *Phys. Rev. Lett.* **86**, 2934–2937 (2001).

52. White, J.A., Rubinstein, J.T. & Kay, A.R. Channel noise in neurons. *Trends Neurosci.* **23**, 131–137 (2000).

53. Branco, T. & Staras, K. The probability of neurotransmitter release: variability and feedback control at single synapses. *Nat. Rev. Neurosci.* **10**, 373–383 (2009).

54. Carandini, M. Amplification of trial-to-trial response variability by neurons in visual cortex. *PLoS Biol.* **2**, e264 (2004).

55. Lee, S.H. & Dan, Y. Neuromodulation of brain states. *Neuron* **76**, 209–222 (2012).

56. Mochol, G., Hermoso-Mendizabal, A., Sakata, S., Harris, K.D. & de la Rocha, J. Stochastic transitions into silence cause noise correlations in cortical circuits. *Proc. Natl. Acad. Sci. USA* **112**, 3529–3534 (2015).

57. Okun, M. & Lampl, I. Instantaneous correlation of excitation and inhibition during ongoing and sensory-evoked activities. *Nat. Neurosci.* **11**, 535–537 (2008).

58. Haider, B., Duque, A., Hasenstaub, A.R. & McCormick, D.A. Neocortical network activity in vivo is generated through a dynamic balance of excitation and inhibition. *J. Neurosci.* **26**, 4535–4545 (2006).

59. Graupner, M. & Reyes, A.D. Synaptic input correlations leading to membrane potential decorrelation of spontaneous activity in cortex. *J. Neurosci.* **33**, 15075–15085 (2013).

60. Miller, K.D., Pinto, D.J. & Simons, D.J. Processing in layer 4 of the neocortical circuit: new insights from visual and somatosensory cortex. *Curr. Opin. Neurobiol.* **11**, 488–497 (2001).

61. Berman, N.J. & Maler, L. Inhibition evoked from primary afferents in the electrosensory lateral line lobe of the weakly electric fish (Apteronotus leptorhynchus). *J. Neurophysiol.* **80**, 3173–3196 (1998).

62. Wehr, M. & Zador, A.M. Balanced inhibition underlies tuning and sharpens spike timing in auditory cortex. *Nature* **426**, 442–446 (2003).

63. Priebe, N.J. & Ferster, D. Direction selectivity of excitation and inhibition in simple cells of the cat primary visual cortex. *Neuron* **45**, 133–145 (2005).

64. Middleton, J.W., Omar, C., Doiron, B. & Simons, D.J. Neural correlation is stimulus modulated by feedforward inhibitory circuitry. *J. Neurosci.* **32**, 506–518 (2012).

65. Ly, C., Middleton, J.W. & Doiron, B. Cellular and circuit mechanisms maintain low spike co-variability and enhance population coding in somatosensory cortex. *Front. Comput. Neurosci.* **6**, 7 (2012).

66. Litwin-Kumar, A., Chacron, M.J. & Doiron, B. The spatial structure of stimuli shapes the timescale of correlations in population spiking activity. *PLoS Comput. Biol.* **8**, e1002667 (2012).

67. Simmonds, B. & Chacron, M.J. Activation of parallel fiber feedback by spatially diffuse stimuli reduces signal and noise correlations via independent mechanisms in a cerebellum-like structure. *PLoS Comput. Biol.* **11**, e1004034 (2015).

68. van Vreeswijk, C. & Sompolinsky, H. Chaotic balanced state in a model of cortical circuits. *Neural Comput.* **10**, 1321–1371 (1998).

69. Tetzlaff, T., Helias, M., Einevoll, G.T. & Diesmann, M. Decorrelation of neural-network activity by inhibitory feedback. *PLoS Comput. Biol.* **8**, e1002596 (2012).

70. Parga, N. Towards a self-consistent description of irregular and asynchronous cortical activity. *J. Stat. Mech.* **2013**, P03010 (2013).

71. Vere-Jones, D. Simple stochastic models for the release of quanta of transmitter from a nerve terminal. *Aust. J. Stat.* **8**, 53–63 (1966).

72. Tsodyks, M., Pawelzik, K. & Markram, H. Neural networks with dynamic synapses. *Neural Comput.* **10**, 821–835 (1998).

73. Fuhrmann, G., Segev, I., Markram, H. & Tsodyks, M. Coding of temporal information by activity-dependent synapses. *J. Neurophysiol.* **87**, 140–148 (2002).

74. de la Rocha, J. & Parga, N. Short-term synaptic depression causes a non-monotonic response to correlated stimuli. *J. Neurosci.* **25**, 8416–8431 (2005).

75. Rosenbaum, R., Rubin, J. & Doiron, B. Short-term synaptic depression imposes a frequency dependent filter on synaptic information transfer. *PLoS Comput. Biol.* **8**, e1002557 (2012).

76. Zucker, R.S. & Regehr, W.G. Short-term synaptic plasticity. *Annu. Rev. Physiol.* **64**, 355–405 (2002).
77. Goldman, M.S. Enhancement of information transmission efficiency by synaptic failures. *Neural Comput.* **16**, 1137–1162 (2004).
78. Rosenbaum, R., Rubin, J.E. & Doiron, B. Short-term synaptic depression and stochastic vesicle dynamics reduce and shape neuronal correlations. *J. Neurophysiol.* **109**, 475–484 (2013).
79. Bird, A.D. & Richardson, M.J. Long-term plasticity determines the postsynaptic response to correlated afferents with multivesicular short-term synaptic depression. *Front. Comput. Neurosci.* **8**, 2 (2014).
80. Cecchi, G.A. *et al.* Noise in neurons is message dependent. *Proc. Natl. Acad. Sci. USA* **97**, 5557–5561 (2000).
81. Faisal, A.A., Selen, L.P. & Wolpert, D.M. Noise in the nervous system. *Nat. Rev. Neurosci.* **9**, 292–303 (2008).
82. Rubinstein, J.T. Threshold fluctuations in an N sodium channel model of the node of Ranvier. *Biophys. J.* **68**, 779–785 (1995).
83. Gal, A. *et al.* Dynamics of excitability over extended timescales in cultured cortical neurons. *J. Neurosci.* **30**, 16332–16342 (2010).
84. Hô, N. & Destexhe, A. Synaptic background activity enhances the responsiveness of neocortical pyramidal neurons. *J. Neurophysiol.* **84**, 1488–1496 (2000).
85. Doiron, B., Longtin, A., Berman, N. & Maler, L. Subtractive and divisive inhibition: effect of voltage-dependent inhibitory conductances and noise. *Neural Comput.* **13**, 227–248 (2001).
86. Hansel, D. & van Vreeswijk, C. How noise contributes to contrast invariance of orientation tuning in cat visual cortex. *J. Neurosci.* **22**, 5118–5128 (2002).
87. Prescott, S.A. & De Koninck, Y. Gain control of firing rate by shunting inhibition: roles of synaptic noise and dendritic saturation. *Proc. Natl. Acad. Sci. USA* **100**, 2076–2081 (2003).
88. Chance, F.S., Abbott, L.F. & Reyes, A.D. Gain modulation from background synaptic input. *Neuron* **35**, 773–782 (2002).
89. Litwin-Kumar, A., Oswald, A.M., Urban, N.N. & Doiron, B. Balanced synaptic input shapes the correlation between neural spike trains. *PLoS Comput. Biol.* **7**, e1002305 (2011).
90. Cardin, J.A., Palmer, L.A. & Contreras, D. Cellular mechanisms underlying stimulus-dependent gain modulation in primary visual cortex neurons in vivo. *Neuron* **59**, 150–160 (2008).
91. Ginzburg, I. & Sompolinsky, H. Theory of correlations in stochastic neural networks. *Phys. Rev. E Stat. Phys. Plasmas Fluids Relat. Interdiscip. Topics* **50**, 3171–3191 (1994).
92. Moreno-Bote, R. & Parga, N. Auto- and crosscorrelograms for the spike response of leaky integrate-and-fire neurons with slow synapses. *Phys. Rev. Lett.* **96**, 028101 (2006).
93. Rosenbaum, R. & Josić, K. Mechanisms that modulate the transfer of spiking correlations. *Neural Comput.* **23**, 1261–1305 (2011).
94. Kruscha, A. & Lindner, B. Spike-count distribution in a neuronal population under weak common stimulation. *Phys. Rev. E* **92**, 052817 (2015).
95. Lyamzin, D.R. *et al.* Nonlinear transfer of signal and noise correlations in cortical networks. *J. Neurosci.* **35**, 8065–8080 (2015).
96. Cohen, M.R. & Maunsell, J.H. Attention improves performance primarily by reducing interneuronal correlations. *Nat. Neurosci.* **12**, 1594–1600 (2009).
97. Galán, R.F., Fourcaud-Trocmé, N., Ermentrout, G.B. & Urban, N.N. Correlation-induced synchronization of oscillations in olfactory bulb neurons. *J. Neurosci.* **26**, 3646–3655 (2006).
98. Barreiro, A.K., Shea-Brown, E. & Thilo, E.L. Time scales of spike-train correlation for neural oscillators with common drive. *Phys. Rev. E* **81**, 011916 (2010).
99. Abouzeid, A. & Ermentrout, B. Correlation transfer in stochastically driven neural oscillators over long and short time scales. *Phys. Rev. E* **84**, 061914 (2011).
100. Hong, S., Ratté, S., Prescott, S.A. & De Schutter, E. Single neuron firing properties impact correlation-based population coding. *J. Neurosci.* **32**, 1413–1428 (2012).
101. Ocker, G.K. & Doiron, B. Kv7 channels regulate pairwise spiking covariability in health and disease. *J. Neurophysiol.* **112**, 340–352 (2014).
102. Burak, Y., Lewallen, S. & Sompolinsky, H. Stimulus-dependent correlations in threshold-crossing spiking neurons. *Neural Comput.* **21**, 2269–2308 (2009).
103. Markowitz, D.A., Collman, F., Brody, C.D., Hopfield, J.J. & Tank, D.W. Rate-specific synchrony: using noisy oscillations to detect equally active neurons. *Proc. Natl. Acad. Sci. USA* **105**, 8422–8427 (2008).
104. Zhou, P., Burton, S.D., Urban, N.N. & Ermentrout, G.B. Impact of neuronal heterogeneity on correlated colored noise-induced synchronization. *Front. Comput. Neurosci.* **7**, 113 (2013).
105. Silver, R.A. Neuronal arithmetic. *Nat. Rev. Neurosci.* **11**, 474–489 (2010).
106. Kass, R.E. & Ventura, V. Spike count correlation increases with length of time interval in the presence of trial-to-trial variation. *Neural Comput.* **18**, 2583–2591 (2006).
107. Ermentrout, B. Neural networks as spatio-temporal pattern-forming systems. *Rep. Prog. Phys.* **61**, 353 (1998).
108. Vogels, T.P., Rajan, K. & Abbott, L.F. Neural network dynamics. *Annu. Rev. Neurosci.* **28**, 357–376 (2005).
109. Gerstner, W., Kistler, W.M., Naud, R. & Paninski, L. *Neuronal Dynamics: From Single Neurons to Networks and Models of Cognition* (Cambridge University Press, 2014).
110. Kopell, N., Ermentrout, G.B., Whittington, M.A. & Traub, R.D. Gamma rhythms and beta rhythms have different synchronization properties. *Proc. Natl. Acad. Sci. USA* **97**, 1867–1872 (2000).
111. Brunel, N. & Wang, X.J. What determines the frequency of fast network oscillations with irregular neural discharges? I. Synaptic dynamics and excitation-inhibition balance. *J. Neurophysiol.* **90**, 415–430 (2003).
112. Hertz, J. Cross-correlations in high-conductance states of a model cortical network. *Neural Comput.* **22**, 427–447 (2010).
113. Bujan, A.F., Aertsen, A. & Kumar, A. Role of input correlations in shaping the variability and noise correlations of evoked activity in the neocortex. *J. Neurosci.* **35**, 8611–8625 (2015).
114. Litwin-Kumar, A. & Doiron, B. Slow dynamics and high variability in balanced cortical networks with clustered connections. *Nat. Neurosci.* **15**, 1498–1505 (2012).
115. Doiron, B. & Litwin-Kumar, A. Balanced neural architecture and the idling brain. *Front. Comput. Neurosci.* **8**, 56 (2014).
116. Schaub, M.T., Billeh, Y.N., Anastassiou, C.A., Koch, C. & Barahona, M. Emergence of slow-switching assemblies in structured neuronal networks. *PLoS Comput. Biol.* **11**, e1004196 (2015).
117. Keane, A. & Gong, P. Propagating waves can explain irregular neural dynamics. *J. Neurosci.* **35**, 1591–1605 (2015).
118. Kriener, B., Helias, M., Aertsen, A. & Rotter, S. Correlations in spiking neuronal networks with distance dependent connections. *J. Comput. Neurosci.* **27**, 177–200 (2009).
119. Ko, H. *et al.* Functional specificity of local synaptic connections in neocortical networks. *Nature* **473**, 87–91 (2011).
120. Kelly, R.C., Smith, M.A., Kass, R.E. & Lee, T.S. Local field potentials indicate network state and account for neuronal response variability. *J. Comput. Neurosci.* **29**, 567–579 (2010).
121. Doiron, B., Lindner, B., Longtin, A., Maler, L. & Bastian, J. Oscillatory activity in electrosensory neurons increases with the spatial correlation of the stochastic input stimulus. *Phys. Rev. Lett.* **93**, 048101 (2004).
122. Lindner, B., Doiron, B. & Longtin, A. Theory of oscillatory firing induced by spatially correlated noise and delayed inhibitory feedback. *Phys. Rev. E* **72**, 061919 (2005).
123. Polk, A., Litwin-Kumar, A. & Doiron, B. Correlated neural variability in persistent state networks. *Proc. Natl. Acad. Sci. USA* **109**, 6295–6300 (2012).
124. Ostojic, S., Brunel, N. & Hakim, V. How connectivity, background activity and synaptic properties shape the cross-correlation between spike trains. *J. Neurosci.* **29**, 10234–10253 (2009).
125. Ostojic, S. Two types of asynchronous activity in networks of excitatory and inhibitory spiking neurons. *Nat. Neurosci.* **17**, 594–600 (2014).
126. Harish, O. & Hansel, D. Asynchronous rate chaos in spiking neuronal circuits. *PLoS Comput. Biol.* **11**, e1004266 (2015).
127. Luo, L., Callaway, E.M. & Svoboda, K. Genetic dissection of neural circuits. *Neuron* **57**, 634–660 (2008).
128. Fenno, L., Yizhar, O. & Deisseroth, K. The development and application of optogenetics. *Annu. Rev. Neurosci.* **34**, 389–412 (2011).
129. Gu, Y. *et al.* Perceptual learning reduces interneuronal correlations in macaque visual cortex. *Neuron* **71**, 750–761 (2011).
130. Romo, R., Hernández, A., Zainos, A. & Salinas, E. Correlated neuronal discharges that increase coding efficiency during perceptual discrimination. *Neuron* **38**, 649–657 (2003).
131. Riehle, A., Grün, S., Diesmann, M. & Aertsen, A. Spike synchronization and rate modulation differentially involved in motor cortical function. *Science* **278**, 1950–1953 (1997).
132. Chacron, M.J. & Bastian, J. Population coding by electrosensory neurons. *J. Neurophysiol.* **99**, 1825–1835 (2008).
133. Mitchell, J.F., Sundberg, K.A. & Reynolds, J.H. Spatial attention decorrelates intrinsic activity fluctuations in macaque area V4. *Neuron* **63**, 879–888 (2009).
134. Ruff, D.A. & Cohen, M.R. Attention can either increase or decrease spike count correlations in visual cortex. *Nat. Neurosci.* **17**, 1591–1597 (2014).
135. Gregoriou, G.G., Rossi, A.F., Ungerleider, L.G. & Desimone, R. Lesions of prefrontal cortex reduce attentional modulation of neuronal responses and synchrony in V4. *Nat. Neurosci.* **17**, 1003–1011 (2014).
136. Gutnisky, D.A. & Dragoi, V. Adaptive coding of visual information in neural populations. *Nature* **452**, 220–224 (2008).
137. Snyder, A.C., Morais, M.J., Kohn, A. & Smith, M.A. Correlations in V1 are reduced by stimulation outside the receptive field. *J. Neurosci.* **34**, 11222–11227 (2014).
138. Herrero, J.L., Gieselmann, M.A., Sanayei, M. & Thiele, A. Attention-induced variance and noise correlation reduction in macaque V1 is mediated by NMDA receptors. *Neuron* **78**, 729–739 (2013).
139. Vinck, M., Batista-Brito, R., Knoblich, U. & Cardin, J.A. Arousal and locomotion make distinct contributions to cortical activity patterns and visual encoding. *Neuron* **86**, 740–754 (2015).
140. Reimer, J. *et al.* Pupil fluctuations track fast switching of cortical states during quiet wakefulness. *Neuron* **84**, 355–362 (2014).
141. Erisken, S. *et al.* Effects of locomotion extend throughout the mouse early visual system. *Curr. Biol.* **24**, 2899–2907 (2014).
142. Downer, J.D., Niwa, M. & Sutter, M.L. Task engagement selectively modulates neural correlations in primary auditory cortex. *J. Neurosci.* **35**, 7565–7574 (2015).
143. Qi, X.L. & Constantinidis, C. Correlated discharges in the primate prefrontal cortex before and after working memory training. *Eur. J. Neurosci.* **36**, 3538–3548 (2012).
144. Cohen, M.R. & Newsome, W.T. Context-dependent changes in functional circuitry in visual area MT. *Neuron* **60**, 162–173 (2008).

145. Miura, K., Mainen, Z.F. & Uchida, N. Odor representations in olfactory cortex: distributed rate coding and decorrelated population activity. *Neuron* **74**, 1087–1098 (2012).

146. Jeanne, J.M., Sharpee, T.O. & Gentner, T.Q. Associative learning enhances population coding by inverting interneuronal correlation patterns. *Neuron* **78**, 352–363 (2013).

147. Biederlack, J. *et al*. Brightness induction: rate enhancement and neuronal synchronization as complementary codes. *Neuron* **52**, 1073–1083 (2006).

148. Yu, J. & Ferster, D. Membrane potential synchrony in primary visual cortex during sensory stimulation. *Neuron* **68**, 1187–1201 (2010).

149. Poulet, J.F. & Petersen, C.C. Internal brain state regulates membrane potential synchrony in barrel cortex of behaving mice. *Nature* **454**, 881–885 (2008).

150. Tan, A.Y., Chen, Y., Scholl, B., Seidemann, E. & Priebe, N.J. Sensory stimulation shifts visual cortex from synchronous to asynchronous states. *Nature* **509**, 226–229 (2014).